Progress In Electromagnetics Research C, Vol. 52, 71–82, 2014

Design of Fragment-Type Isolation Structures for MIMO Antennas

Lu Wang[1], Gang Wang[1, 2, *], and Johan Sidén[3]

Abstract—Fragment structure should find its application in acquiring high isolation between multiple-input multiple-output (MIMO) antennas. By gridding a design space into fragment cells, a fragment-type isolation structure can be constructed by metalizing some of the fragment cells. For MIMO isolation design, cells to be metalized can be selected by optimization searching scheme with objectives such as isolation, return losses, and even radiation patterns of MIMO antennas. Due to the flexibility of fragment-type isolation structure, fragment-type structure has potentials to yield isolation higher than canonical isolation structures. In this paper, multi-objective evolutionary algorithm based on decomposition combined with genetic operators (MOEA/D-GO) is applied to design fragment-type isolation structures for MIMO patch antennas and MIMO PIFAs. It is demonstrated that isolation can be improved to different extents by using fragment-type isolation design. Some technique aspects related to the fragment-type isolation design, such as effects of fragment cell size, design space, density of metal cells, and efficiency consideration, are further discussed.

1. INTRODUCTION

Multiple-input and multiple-output (MIMO) technique shows great potentials in wireless communication. In a MIMO system with antennas deployed in tight space, mutual coupling could be strong enough to degrade the performance of MIMO system [1, 2]. To achieve low mutual coupling or high isolation between closely-deployed MIMO antennas is a key challenge in MIMO design.

Various structures have been designed to suppress mutual coupling between MIMO antennas. These designs include the use of parasitic elements [3], vias [4], electromagnetic bandgap structures [5], slots [6, 7], resonator structure [8], meta-surface [9], metamaterial structure [10, 11], and some other structures [12–14]. It should be noted although the reported isolation structures have different forms or shapes, they were basically designed in terms of canonical structures. In practice, there are some limitations in such design even though canonical structures can be optimized. First, there is no guarantee that a canonical structure, although optimized, is the best for structure in a design space to produce isolation high as possible. Second, canonical structures usually have limited flexibility so that it may be hard to arrange them in a compact design space of specific shape. Therefore, structures with higher isolation and more flexibility for deployment in MIMO system are highly desired.

Fragment-type structure has the desired flexibility to suit any design space. As shown in Fig. 1, an irregular design space can always be gridded into cells, and the cells can be assigned with either "1" or "0". A fragment-type structure can be constructed by assigning "1" and "0" to metal cell and non-metal cell, respectively. Obviously, such fragment-type isolation structure has great flexibility for fitting space of arbitrary shape left in a MIMO system for isolation design.

Fragment-type structure has been proposed for antenna design for years [15–20]. It is generally noted that fragment-type antennas may provide great convenience for impedance matching and

Received 15 May 2014, Accepted 13 July 2014, Scheduled 18 July 2014

* Corresponding author: Gang Wang (gwang01@ustc.edu.cn).

[1] Department of Electronic Engineering and Information Science, University of Science and Technology of China, Hefei 230027, China. [2] Key Laboratory of Electromagnetic Space Information, Chinese Academy of Sciences, Hefei 230027, China. [3] Department of Electronics Design, Mid Sweden University, Sundsvall SE-851 70, Sweden.

broadband operation [19, 20]. However, there seems no report on the design of isolation structure with fragment-type structures.

Fragment-type structure should find its application in antenna isolation design. In this paper, we will propose fragment-type isolation structure for MIMO antennas and its design techniques. In Section 2, we will give a brief description of MOEA/D-GO for fragment-type isolation structure design. In Section 3, two design examples with fragment-type isolation structures for MIMO systems with patch antennas and PIFA antennas are reported for verification. In Section 4, some technique aspects related to fragment-type isolation design, such as effects of fragment cell size and isolation design space, are further discussed. It is shown that designs with the proposed fragment-type structures have potential to acquire isolation higher than that with canonical structures.

2. MOEA/D-GO FOR FRAGMENT-TYPE ISOLATION STRUCTURE DESIGN

2.1. Design Matrix for Fragment-Type Isolation

As shown in Fig. 1, a fragment-type structure can be defined by gridding a specified design space into cells assigned with "1" and "0", and metalizing those cells assigned with "1". According to the distribution of "1" and "0", a design matrix can be constructed to denote the fragment-type isolation structure, in a straightforward sequence or other specified sequence.

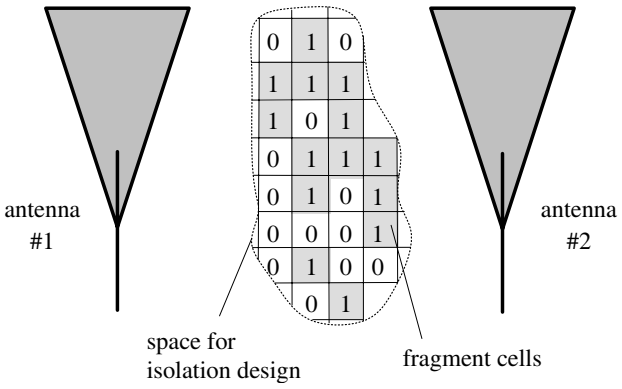

Figure 1. Fragment-type isolation structure for MIMO system.

Once a design matrix is constructed, the design of fragment-type isolation structure is transformed to seek a proper design matrix to achieve isolation as high as possible in the operation frequency bandwidth.

2.2. MOP for Fragment-Type MIMO Isolation Design

Proper design matrix can be obtained by using optimization searching techniques. Genetic algorithm (GA) may be the most well-known for optimization of fragment-type structure [19, 20]. The GA coding representation for discrete parameters, viz., the 0-1 character string, suits well for fragment-type structure as shown in Fig. 1. Moreover, GA can search across a wide sampling of the solution space, and handle a large number of variables.

In general, MIMO isolation design is a multi-objective optimization problem (MOP) rather than a single-objective optimization problem. The reason is that, for MIMO antenna isolation design, characteristics such as isolation, return losses, gains and even radiation patterns of MIMO antennas should be guaranteed.

To solve MOP for fragment-type design, a high-efficiency multiobjective optimization technique for fragmented antenna design, referred to as multiobjective evolutionary algorithm based on decomposition with genetic operators (MOEA/D-GO) [21], can be applied. The MOEA/D-GO carries forward all advantages of MOEA/D and GA.

For MIMO antenna isolation design as shown in Fig. 1, the MOP can be defined as

$$\begin{aligned} &\text{minimize } F(x) = (f_1(x), f_2(x), \ldots, f_m(x)), \\ &\text{subject to } x \in \Omega, \end{aligned} \tag{1}$$

where functions $f_i(x)$ $(i = 1, 2, \ldots, m)$ represent m objectives such as return loss, isolation, gain, etc. Ω is a decision space, and x is a decision variable which defines a fragment-type isolation structure.

In terms of -10 dB return loss and desired isolation Q (in dB), the objective functions in (1) for isolation design of 2×2 MIMO can be specified as

$$f_i(x) = \max\left(10 - \min_{\omega\in[\omega_1,\omega_2]} |S_{ii}|_{\text{dB}}, 0\right) \quad (i = 1, 2), \tag{2}$$

$$f_3(x) = \max\left(Q - \min_{\omega\in[\omega_1,\omega_2]} |S_{21}|_{\text{dB}}, 0\right) \tag{3}$$

where $[\omega_1, \omega_2]$ characterizes the operation band of MIMO system, $|S_{ii}|_{\text{dB}}\,(i = 1, 2)$ indicate the corresponding return losses of two MIMO antennas, $|S_{21}|_{\text{dB}}$ indicates the isolation between the two MIMO antennas.

Multiple objective functions are quite reasonable for MIMO isolation design. In fact, the equivalent circuit 2×2 of MIMO yields

$$|S_{11}|^2 + |S_{21}|^2 = 1 - \delta \quad (\delta > 0), \tag{4}$$

where δ represents losses (including the radiation loss).

Judging from (4), $|S_{11}|$ and $|S_{21}|$ are correlated to some extent, and it seems that to acquire a small return loss (small $|S_{11}|$) and to acquire a high isolation (small $|S_{21}|$) are contradictory. However, (4) represents a dynamic constrain because different isolation structures will yield different δ. For a fixed small $|S_{11}|$, there may be different values of $|S_{21}|$ for different isolation structures. In fact, multiobjective optimization will find its application if there are objectives being contradictory.

The use of fragment-type structures in isolation design provides the possibility to seek structures of isolation as high as possible. To this aim, we may set a value of Q in (3) being much larger than a desired isolation (e.g., $Q = 100$). The MOEA/D-GO scheme will start to search for a design matrix to approach to this very large Q.

It should be remarked that large Q may lead to unending optimization search searching in MOEA/D-GO within a bearable design period. For this scenario, we can check the acquired isolation to see if there is a need to terminate the searching manually. For the design examples in this paper, Q is set to be 50 dB.

In fragment-type MIMO isolation design, MOEA/D-GO scheme must be combined with electromagnetic simulation. The optimization kernel is constructed by using MOEA/D-GO and EM simulator. In our design in this paper, MOEA/D-GO is implemented by using Visual C++ 6.0, and using HFSS as simulator. The overall computational cost is mainly determined by EM simulation.

3. FRAGMENT-TYPE ISOLATION STRUCTURE DESIGN FOR PATCH ANTENNAS AND PIFAS

For demonstration, we will apply the proposed fragment-type isolation structure design technique to MIMO patch antennas and PIFAs. This design technique can also be tested with other MIMO antennas.

3.1. Fragment-Type Isolation for MIMO Patches

Geometry of two closely-packed MIMO patch antennas on a metal ground plane is shown in Fig. 2. Antennas are printed on FR4 PCB (dielectric substrate of thickness $h = 1.6$ mm and relative permittivity of 4.4) with $w1 = 75$ mm, $w2 = 17.5$ mm, $L1 = 61$ mm, $d = 21$ mm, $w = 120$ mm, and $L = 197$ mm. The MIMO patches share a ground plate of 120 mm $\times$ 197 mm.

Typical MIMO isolation design for the patch antennas was carried out with slots of canonical shape on the ground plate in the area as shown in Fig. 2. It was reported that isolation of approximate 27 dB can be achieved by designing isolation slots in design space of 120 mm $\times$ 21 mm on the ground plane [6].

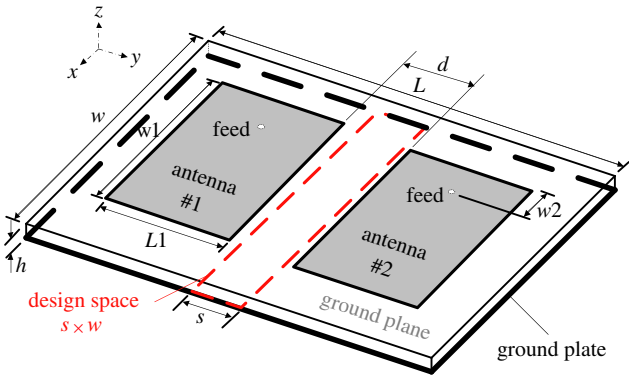

Figure 2. Geometry of two closely-packed patch antennas.

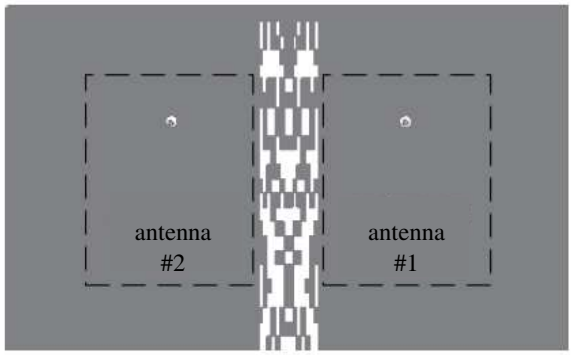

Figure 3. Layout of fragment-type isolation structure on the ground plane for two closely-packed patch antennas.

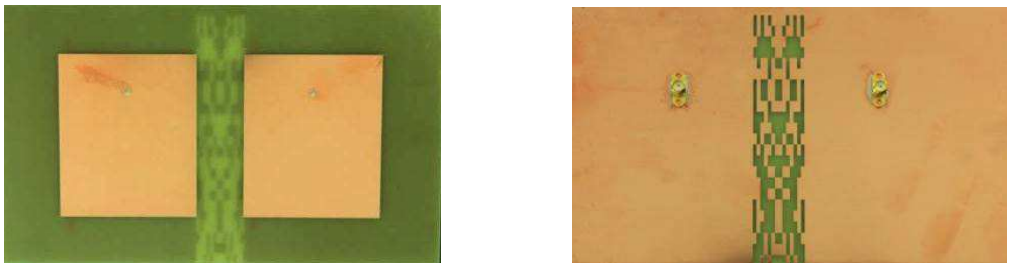

(a) (b)

Figure 4. Prototype of MIMO patch antennas with fragment-type isolation structure on the ground plate. (a) MIMO patches. (b) Isolation fragments.

For our fragment-type isolation structure design, we take the same design space on the ground plane as used in [6]. After gridding the design space with cell size of $dx \times dy = 5\,\text{mm} \times 1.5\,\text{mm}$, and implementing the MOEA/D-GO optimization as in section 2, 4 candidate fragment-type structures can be obtained in terms of isolation higher than 35 dB. One of the fragment-type isolation structures is shown in Fig. 3.

A prototype MIMO patches with fragment-type isolation in Fig. 3 is fabricated. Fig. 4 shows MIMO patch antennas with fragment-type isolation on the ground plane.

For the prototype MIMO patch antennas, the simulated and measured return losses (characterized by $|S_{11}|$) and isolation between the two patches (characterized by $|S_{21}|$) are depicted in Fig. 5. We find good agreement between the simulated results and test results. From Fig. 5, it is observed that there is a simulated isolation of 47 dB at 0.94 GHz, and a measured isolation of 37 dB at 0.94 GHz. Compared to the isolation acquired with slots on the ground [6], the measured isolation has been increased by 10 dB. Meanwhile, we observed that the measured isolation shifts a little to higher frequency compared to the simulated result.

To show more about the mechanism of isolation, Fig. 6 depicts the current distribution on the surface of ground plate when one of the patch antennas (antenna #2) is excited and the other (antenna #1) is terminated by matching impedance. We find in Fig. 6 that, a large portion of surface current is trapped by the isolation structure. Therefore, the fragment-type structure may substantially reduce mutual coupling between the two patch antennas, and provide an efficient isolation between the two MIMO patch antennas.

To evaluate the performance of MIMO system with patch antennas in Fig. 4, we may calculate the envelope correlation coefficient ρ_e. Under the assumption of uniform multipath environment, ρ_e of a

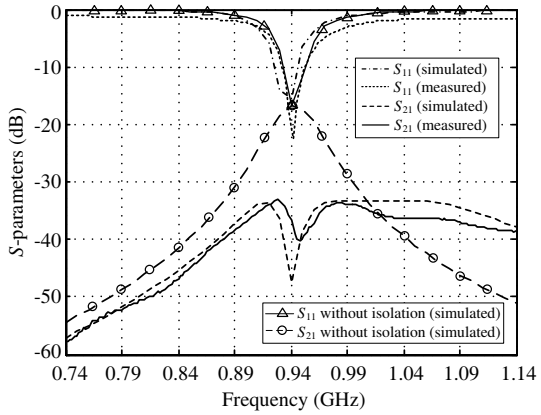

Figure 5. Simulated and measured return loss and isolation of the MIMO patch antennas with fragment-type isolation structure.

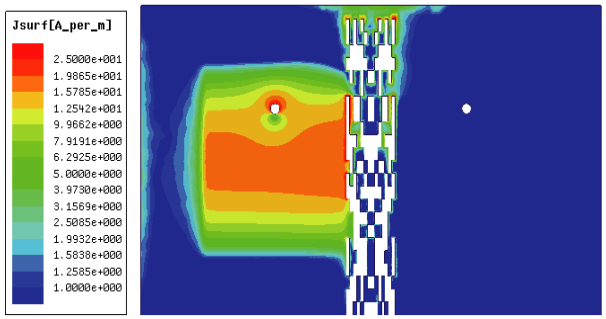

Figure 6. Surface current distribution on the ground plane of MIMO patches.

two antennas MIMO system can be determined using the following equation [22]

$$\rho_e = \frac{\left|S_{11}^* S_{12} + S_{21}^* S_{22}\right|^2}{\left(1 - \left(|S_{11}|^2 + |S_{21}|^2\right)\right)\left(1 - \left(|S_{22}|^2 + |S_{12}|^2\right)\right)} \tag{5}$$

Figure 7(a) shows the variation of ρ_e versus frequency for the MIMO system with patch antennas in Fig. 4. For comparison, for MIMO system without antenna isolation design is also depicted. It is observed that MIMO patches with fragment-type isolation structure yield approximately zero values fo ρ_e rat 0.94 GHz, which indicates perfect decorrelation between the MIMO antenna elements.

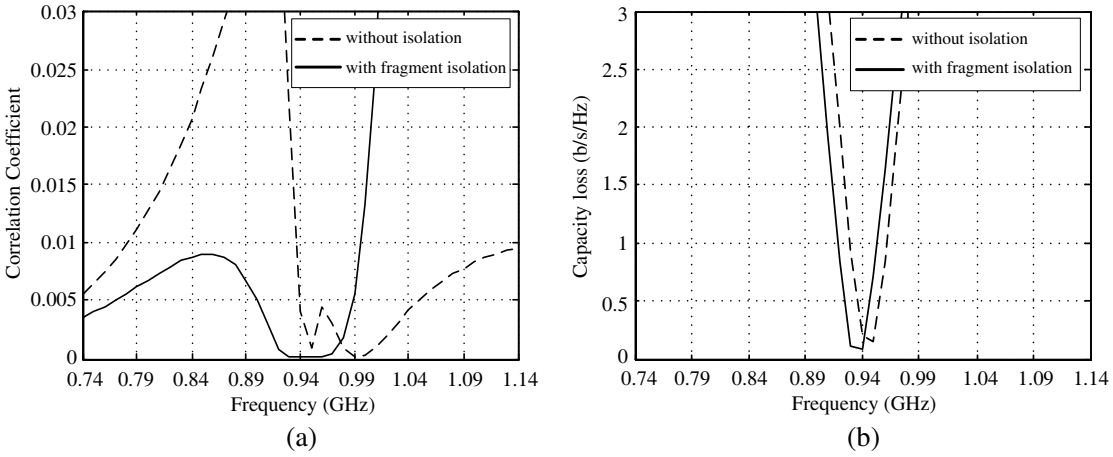

Figure 7. MIMO system characteristics with the designed MIMO patches. (a) Correlation coefficient. (b) Capacity loss.

In the presence of uncorrelated Rayleigh-fading MIMO channels, channel capacity will suffer some losses, which can be computed from the correlation matrices [23]. For a 2×2 MIMO system, in case that only the receiving antennas are correlated and high SNR is occurred, the capacity loss C_{loss} can be evaluated as [24]

$$C_{\text{loss}} = -\log_2 \det\left(\Phi^R\right) \tag{6}$$

where Φ^R is correlation matrix of receiving antennas and can be given by

$$\Phi^R = \begin{bmatrix} \phi_{11} & \phi_{12} \\ \phi_{21} & \phi_{22} \end{bmatrix} \tag{7}$$

with $\phi_{ii} = 1 - (|S_{ii}|^2 + |S_{ij}|^2)$ and $\phi_{ij} = (S_{ii}^* S_{ij} + S_{ji}^* S_{jj})$ (for i, $j = 1$ or 2).

Figure 7(b) shows the variation of C_{loss} versus frequency for the MIMO system with patch antennas in Fig. 4. For comparison, C_{loss} for MIMO system without antenna isolation design is also depicted. We find that that our MIMO antenna design leads to low capacity loss.

3.2. Fragment-Type Isolation for MIMO PIFAs

To illustrate the versatility and superiority of our proposed method, we also apply it to design fragment-type isolation for the closely-packed MIMO PIFAs in [6].

Geometry of the MIMO PIFAs is shown in Fig. 8. The two PIFAs share a common ground plate with an inter-antenna spacing (center to center) $d = 15\,\text{mm}$, $g = 43\,\text{mm}$, $a = 26\,\text{mm}$, $b = 5\,\text{mm}$, $d1 = 2\,\text{mm}$, $d2 = 3\,\text{mm}$, and $h = 6\,\text{mm}$. The design space on the ground for isolation structure design is $43\,\text{mm} \times 10\,\text{mm}$ between the two PIFAs. It was reported that approximate 20 dB isolation can be achieved by using isolation slots in the design space on ground plane [6]. By implementing the MOEA-GO-based design in Section 2, fragment-type isolation structures can be designed. After gridding the design space with cell size of $dx \times dy = 1\,\text{mm} \times 1\,\text{mm}$, and implementing the MOEA/D-GO optimization, 6 candidate fragment-type isolation structures can be acquired for isolation higher than 25 dB. One of the fragment-type isolation structures on the ground plane is depicted in Fig. 9.

A prototype MIMO PIFAs with fragment-type isolation in Fig. 9 is fabricated. Fig. 10 shows the prototype MIMO PIFAs with fragment-type isolation structure on the ground plane. It should be

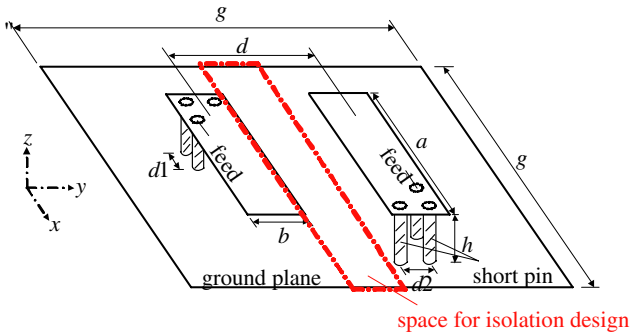

Figure 8. Geometry of two closely-packed PIFAs.

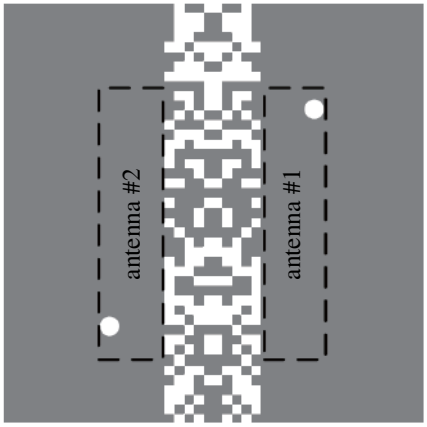

Figure 9. Layout of fragment-type isolation structure on the ground plane for two closely-packed PIFAs.

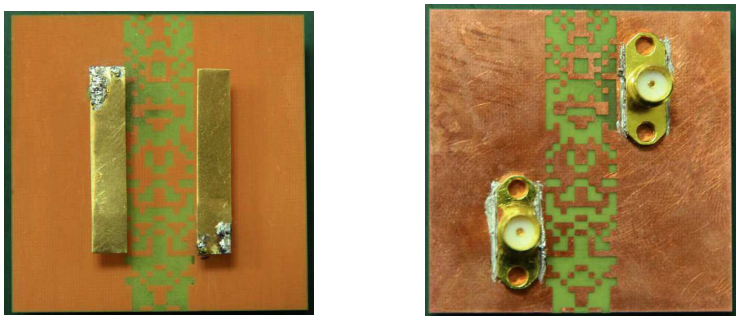

(a) (b)

Figure 10. Prototype of MIMO PIFAs with fragment-type isolation structure on the ground plane. (a) MIMO PIFA arms. (b) Isolation fragments on the ground.

remarked that to support the fragment cells, we have used single-side PCB with dielectric thickness of 0.3 mm and relative permittivity of 2.2.

Figure 11 shows the simulated and measured return losses (characterized by $|S_{11}|$) and isolation between the two patches (characterized by $|S_{21}|$) for the prototype MIMO PIFAs. From the results shown in Fig. 11, we have the observation that the maximum simulated isolation is 47 dB at 2.35 GHz, and the simulated isolation across the band 2.32 GHz $\sim$ 2.39 GHz is higher than 26.4 dB. The measured isolation across the band 2.32 GHz $\sim$ 2.39 GHz is higher than 23.4 dB, and the maximum measured isolation is 48 dB at 2.38 GHz. Meanwhile, the measured impedance bandwidth (in terms of $|S_{11}|$ less than -10 dB) is extended to 2.32 GHz $\sim$ 2.46 GHz. Compared to the measured isolation with slots on the ground in [6], the isolation has been increased by 3.4 dB at least.

To show more about the mechanism of isolation, Fig. 12 depicts the current distribution on the surface of ground plate when one of the PIFAs is excited and the other is terminated by matching impedance. We find that in Fig. 12, a large portion of surface current is trapped by the isolation structure. Therefore, the fragment-type structure may substantially reduce mutual coupling between the two PIFAs, and provide an efficient isolation between the two MIMO PIFAs.

To evaluate performance of MIMO system with MIMO PIFAs in Fig. 10, envelope correlation

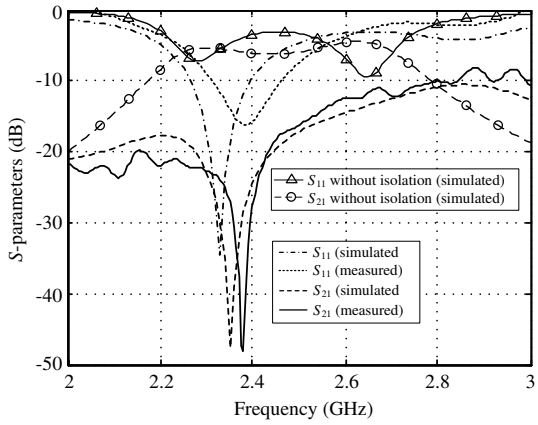

Figure 11. Simulated and measured return loss and isolation of the MIMO PIFAs with fragment-type isolation structure.

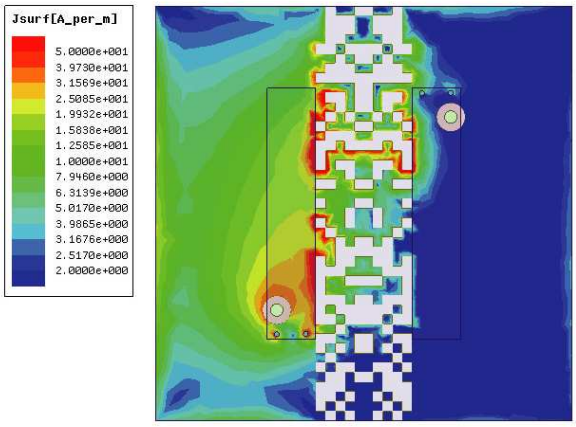

Figure 12. Surface current distribution on the ground plane of MIMO PIFAs.

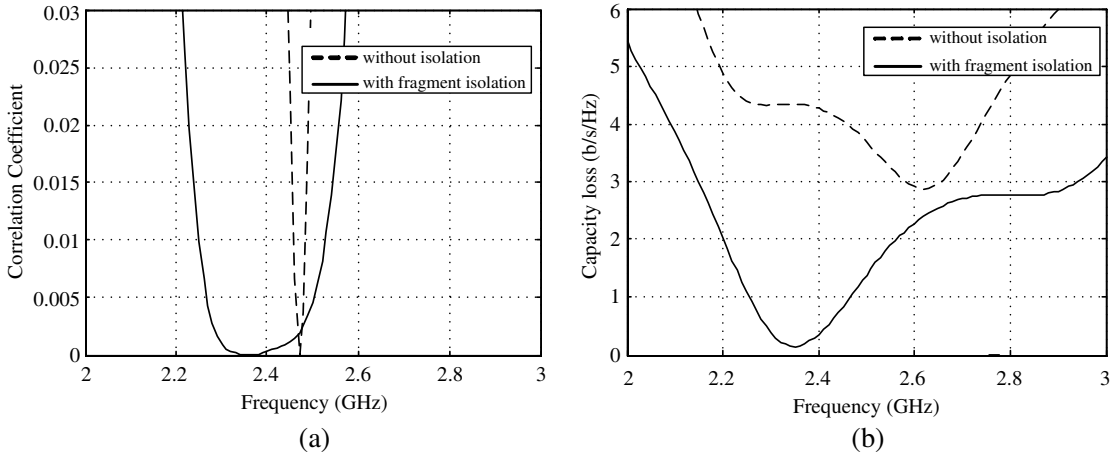

Figure 13. MIMO system characteristics with the designed MIMO PIFAs. (a) Correlation coefficient. (b) Capacity loss.

coefficient ρ_e and capacity loss C_{loss} have been also calculated. Fig. 13(a) shows the variation of envelope correlation coefficient across the desired operating frequency band. Fig. 13(b) depicts the capacity loss. For comparison, both ρ_e and C_{loss} for MIMO PIFA system without antenna isolation design are also depicted.

From Fig. 13(a), we find that MIMO PIFAs with fragment-type isolation structure attain approximately zero values for ρ_e in the frequency band of interest. From Fig. 13(b), we find that that our MIMO PIFA isolation design leads to low capacity loss.

4. FURTHER DISCUSSION

Although higher isolation can be acquired by using fragment-type isolation structure, there are still several problems should be addressed here.

4.1. Different Effects on Radiation Patterns

Strictly speaking, introduction of isolation structure will have some impacts on the radiation patterns of MIMO antennas. Different isolation structures will have different influence on the MIMO radiation pattern.

Figure 14 depicts the impacts of fragment-type isolation structures on normalized gain patterns of MIMO patches at 0.94 GHz (Fig. 14(a)) and MIMO PIFAs at 2.36 GHz (Fig. 14(b)). For comparison, gain patterns without any isolation structure are also depicted. The normalized gain patterns are obtained by feeding patch antenna #1 and loading patch antenna #2 with a matched load.

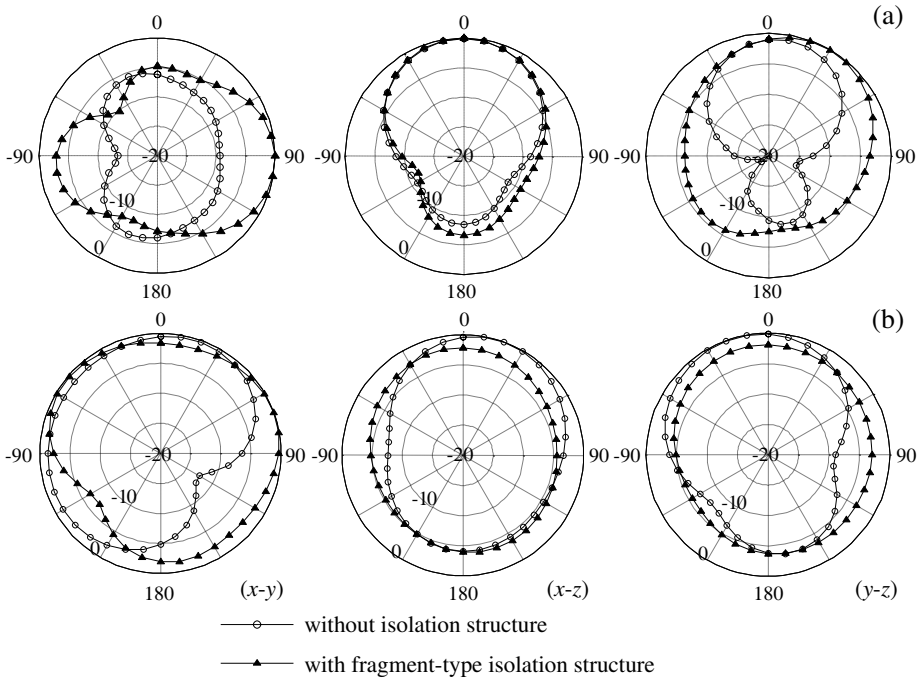

Figure 14. Normalized gain radiation patterns of two closely-packed MIMO antennas. (a) Patch antennas at 0.94 GHz. (b) PIFAs at 2.36 GHz.

From Fig. 14, we find that the fragment-type isolation structure design maintains the maximum radiation along z-direction, although the isolation structure designs tend to expand the patterns more in y-direction.

However, we remark that the radiation efficiency of MIMO patch antennas and MIMO PIFAs with fragment-type isolation is approximately 30.5% and 98.8%. While the radiation efficiency without any

isolation is approximately 19.1% and 29.4%, respectively. The increase of radiation efficiency is primarily due to the reduced mutual coupling between the two antennas after isolation design. It should be noted that the etched fragment cells in space for isolation design on ground plane will introduce backward radiation, which can be controlled by properly setting the metal-cell density.

In case the radiation pattern is seriously damaged that the MIMO system does not work properly, it could be a hard problem for isolation design without using multi-objective optimization techniques. With the MOEA/D-GO, radiation pattern can be readily treated by including it in the MOP objective functions in (1).

4.2. Effects of Fragment Cell Size

Theoretically, if the fragment cell size is small enough, the design scheme defined in Section 2 will provide the best isolation structure for a specified design space. However, too small fragment cell size will lead to a too large searching space for MOEA/D-GO that MOP solution can hardly be solved within a tolerable design period.

Table 1 shows the isolation for MIMO patches with fragment-type isolation structures of different fragment cell sizes in a fixed design space of 120 mm × 14 mm on the ground plane. We have the observation that fragment-type isolation structures designed with smaller cell size tend to provide better isolation.

Table 1. Isolation for different fragment cell sizes.

Fragment cell size $dx \times dy$ (mm)	Isolation at 0.94 GHz (dB)
3×1	30.7
3×1.5	31.7
4×1	26.6
4×1.5	28.8
5×1	23.9
5×1.5	24.9

However, the MOEA/D-GO based isolation design with fragment cell size of $dx \times dy = 3\,\text{mm} \times 1\,\text{mm}$ took about 20 days while the design with fragment cell size of $dx \times dy = 5\,\text{mm} \times 1.5\,\text{mm}$ took about 14 days when the design ran on computer with Intel Core 2 @ 2.99 GHz.

More design simulations indicate that for fragment cell sizes smaller in just one dimension, as shown in Table 1, there may be no significant improvement in the isolation. Therefore, a moderate fragment cell size should be selected if the computer cost is a key consideration.

4.3. Effects of Design Space

Design space plays key role in fragment-type isolation design. Generally, larger space for isolation structure design tends to guarantee higher isolation. In fact, there is only very limited space left for isolation design in most mobile MIMO systems. In our design, we restrict the design space in our fragment-type design to be smaller than the space between the two MIMO patches, i.e., we will keep $s \leq d$ in Fig. 2.

Table 2 lists isolation of MIMO patches with different design space and cell sizes. From Table 2, we have the observation that small design space will lead to low isolation. However, we can still use small fragment cells for small design space to yield high isolation.

4.4. Effects of Density of Metal Cells

In addition to the design space on ground plate, the density of metal cell in the design space may be another concern. For demonstration, we take design space of $w \times s = 120\,\text{mm} \times 21\,\text{mm}$ for MIMO patchs, and fragment cell size of $dx \times dy = 5\,\text{mm} \times 1.5\,\text{mm}$. Thus we have $24 \times 14 = 336$ cells in total.

Table 2. Isolation for different design spaces and fragment cells.

Design space $x \times y$ (mm)	Fragment cell size $dx \times dy$ (mm)	Isolation at 0.94 GHz (dB)
120×14	3×1	30.7
120×14	5×1.5	24.9
120×21	5×1.5	47

Table 3. Isolation for different metal cell densities.

Number of metal cells	Density	Isolation at 0.94 GHz (dB)
0	0%	16.4
128	38%	19
146	43.4%	25.4
154	46%	47
182	54.2%	36
194	57.7%	38
202	60.1%	30.3
236	70.2%	27.1

Table 3 list some of the optimized MIMO patchs isolaiton for different metal cell density. In the design, we assign different numbers of metal cells in the MOEA/D scheme. The density is thus the ratio of number of metal cells to number of total cells (viz., 336).

From Table 3, we find that the best isolation tend to occur at metal cell density around 50%. Using more or less metal cells in design will reduce the isolation.

4.5. Efficiency Consideration

Although using larger design space and smaller fragment cell size will yield higher isolation, there should be some compromise if we consider the searching efficiency of MOEA/D-GO.

Due to the stochastic searching of MOEA/D-GO, statistical result will be better to give a general conclusion about the effects of design space and fragment cell size. For MOEA/D-GO, number of generation can be used to indicate the searching efficiency.

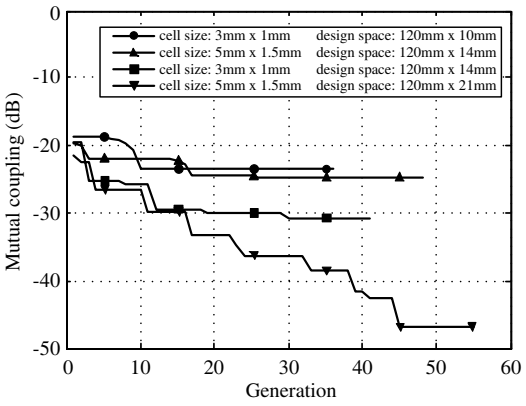

Figure 15. Tendency of isolation in terms of generation number for different design space and cell sizes.

Figure 15 shows the tendency of isolation in the MOEA/D-GO for MIMO patches in terms of number of generation for different design space and cell sizes. For these tests, we have set $Q = 50$ in MOEA/D-GO. From Fig. 15, we have a general view on how the MOEA/D-based searching approaches to its solution.

5. CONCLUSIONS

Fragment-type structure is a promising isolation structure for reducing mutual coupling between closely-packed MIMO antennas. Due to its flexibility, fragment-type isolation structure can be considered especially for scenarios that a design space left for isolation structure does not support canonical isolation structures.

In fragment-type isolation structure design, no presupposed information about the isolation design is required. A satisfactory suppression of mutual coupling between MIMO antennas can always be achieved. But the searching of the best isolation structure for highest isolation achievable within a specified design space is still a big challenge.

Although using larger design space and smaller fragment cell size will yield higher isolation, there should be some compromise if we consider the searching efficiency of MOEA/D-GO.

ACKNOWLEDGMENT

This work was supported in part by National Natural Science Foundation of China under Grant 61272471.

REFERENCES

1. Clerckx, B., C. Craeye, D. Vanhoenacker-Janvier, and C.Oestges, "Impact of antennas coupling on 2×2 MIMO communications," *IEEE Trans. Veh. Technol.*, Vol. 56, No. 3, 1009–1018, May 2007.
2. Bialkowski, M. E., P. Uthansakul, K. Bialkowski, and S. Durrani, "Investigating the performance of MIMO systems from an electromagnetic perspective," *Microw. Opt. Tech. Lett.*, Vol. 48, No. 7, 1233–1238, Jul. 2006.
3. Li, Z., Z. Du, M. Takahashi, K. Saito, and K. Ito, "Reducing mutual coupling of MIMO antennas with parasitic elements for mobile terminals," *IEEE Trans. Antennas Propag.*, Vol. 60, No. 4, 473–481, Feb. 2012.
4. Sarrazin, J., Y. Mahe, S. Avrillon, and S. Toutain, "Collocated microstrip antennas for MIMO systems with a low mutual coupling using mode confinement," *IEEE Trans. Antennas Propag.*, Vol. 58, No. 2, 589–592, Feb. 2010.
5. Yang, F. and Y. Rahmat-Smaii, "Microstrip antennas integrated with electromagnetic band-gap (EBG) structures: A low mutual coupling design for array application," *IEEE Trans. Antennas Propag.*, Vol. 51, No. 10, 2936–2946, Oct. 2003.
6. Chiu, C. Y., C. H. Cheng, R. D. Murch, and C. R. Rowell, "Reduction of mutual coupling between closely-packed antenna elements," *IEEE Trans. Antennas Propag.*, Vol. 55, No. 6, 1732–1738, Jun. 2007.
7. Ouyang, J., F. Yang, and Z. M. Wang, "Reducing mutual coupling of closely spaced microstrip MIMO antennas for WLAN application," *IEEE Antennas Wirel. Propag. Lett.*, Vol. 10, 310–313, 2011.
8. Bait-Suwailam, M. M., O. F. Siddiqui, and O. M. Ramahi, "Mutual coupling reduction between microstrip patch antennas using slotted-complementary split-ring resonators," *IEEE Antennas Wirel. Propag. Lett.*, Vol. 9, 876–878, 2010.
9. Saenz, E., I. Ederra, R. Gonzelo, S. Pivnenko, O. Breinbjerg, and P. de Maggt, "Coupling reduction between dipole antenna elements by using a planar meta-surface," *IEEE Trans. Antennas Propag.*, Vol. 57, No. 2, 383–394, Feb. 2009.

10. Bait-Suwailam, M. M., M. S. Boybay, and O. M. Ramahi, "Electromagnetic coupling reduction in high-profile monopole antennas using single-negative magnetic metamaterials for MIMO applications," *IEEE Trans. Antennas Propag.*, Vol. 58, No. 9, 2894–2902, Sep. 2010.
11. Zhu, J., M. A. Antoniades, and G. V. Eleftheriades, "A compact tri-band monopole antenna with single-cell metamaterial loading," *IEEE Trans. Antennas Propag.*, Vol. 58, No. 4, 1031–1038, Apr. 2010.
12. Gao, Y., X. Chen, Z. Ying, and C. Parini, "Design and performance investigation of a dual-element PIFA array at 2.5 GHz for MIMO terminal," *IEEE Trans. Antennas Propag.*, Vol. 55, No. 9, 3433–3441, Dec. 2007.
13. Dumanli, S., C. J. Railton, and D. L. Paul, "A slot antenna array with low mutual coupling for use on small mobile terminals," *IEEE Trans. Antennas Propag.*, Vol. 59, No. 5, 1512–1520, May 2011.
14. Zhang, S., B. K. Lau, Y. Tan, Z. Ying, and S. He, "Mutual coupling reduction of two PIFA with a T-shape slot impedance transformer for MIMO mobile terminals," *IEEE Trans. Antennas Propag.*, Vol. 60, No. 3, 1521–1531, Mar. 2012.
15. Choo, H., A. Hutani, L. C. Trintinalia, and H. Ling, "Shape optimisation of broadband microstrip antennas using genetic algorithm," *Electron. Lett.*, Vol. 36, 2057–2058, Dec. 2000.
16. Herscovici, N., M. Osorio, and C. Peixeiro, "Miniaturization of rectangular microstrip patches using genetic algorithms," *IEEE Antennas Wirel. Propag. Lett.*, Vol. 1, 94–97, Jan. 2002.
17. Pringle, L. N., P. H. Harms, S. P. Blalock, G. N. Kiesel, E. J. Kuster, P. G. Friederich, R. J. Prado, J. M. Morris, and G. S. Smith, "A reconfigurable aperture antenna based on switched links between electrically small metallic patches," *IEEE Trans. Antennas Propag.*, Vol. 52, 1434–1445, Jun. 2004.
18. Ethier, J., D. McNamara, M. Chaharmir, and J. Shaker, "Reflectarray design using similarity-shaped fragmented sub-wavelength elements," *Electron. Lett.*, Vol. 48, 900–902, 2012.
19. Soontornpipit, P., C. M. Furse, and Y. C. Chung, "Miniaturized biocompatible microstrip antenna using genetic algorithm," *IEEE Trans. Antennas Propag.*, Vol. 53, 1939–1945, Jun. 2005.
20. John, M. and M. Ammann, "Wideband printed monopole design using a genetic algorithm," *IEEE Antennas Wirel. Propag. Lett.*, Vol. 6, 447–449, 2007.
21. Ding, D. and G. Wang, "MOEA/D-GO for fragmented antenna design," *Progress In Electromagnetics Research M*, Vol. 33, 1–15, 2013.
22. Blanch, S., J. Romeu, and I. Corbell, "Exact representation of antenna system diversity performance from input parameter description," *Electron. Lett.*, Vol. 39, No. 9, 705–707, May 2003.
23. Shin, H. and J. H. Lee, "Capacity of multiple-antenna fading channels: Spatial fading correlation, double scattering, and keyhole," *IEEE Trans. Inform. Theory*, Vol. 49, No. 10, 2636–2647, Oct. 2003.
24. Chae, S. H., S.-K. Oh, and S.-O. Park, "Analysis of mutual coupling correlations, and TARC in WiBro MIMO array antenna," *IEEE Antennas Wirel. Propag. Lett.*, Vol. 6, 122–125, 2007.